Valence-band spectra and electronic structure of $CuFeO_2$

V. R. Galakhov, A. I. Poteryaev, E. Z. Kurmaev, and V. I. Anisimov
Institute of Metal Physics, Russian Academy of Sciences, Ural Division, 620219 Yekaterinburg GSP-170, Russia

St. Bartkowski and M. Neumann
University of Osnabrück, Fachbereich Physik, D-49069 Osnabrück, Germany

Z. W. Lu and B. M. Klein
Department of Physics, University of California, Davis, California 95616-8677

Tong-Rong Zhao
Institute for Solid State Physics, University of Tokyo, 7-22-1, Roppongi, Minato-ku, Tokyo 106, Japan
(Received 3 December 1996)

The delafossite-type $CuFeO_2$ single crystal was studied by means of x-ray emission and x-ray photoelectron spectroscopy. The valence state of Cu ions was found to be $1+$, whereas Fe ions were found to be trivalent in the high-spin $S=5/2$ state. The x-ray emission (Cu L_α, Fe L_α, and O K_α) and photoelectron spectra were compared to the results of the local spin density approximation (LSDA) (full-potential linearized augmented plane wave method and linearized muffin-tin orbitals in atomic sphere approximation method) and LSDA $+U$ calculations. It is found that the maximum of the Cu $3d$ state distribution is localized closer to the Fermi level than that of the Fe $3d$ states. The LSDA calculations contradict the experimental results and do not give a correct description of the Cu and Fe $3d$ positions relative to the Fermi level, and incorrectly predict metallic behaviors (semiconductor observed) and give qualitatively incorrect magnetic properties of $CuFeO_2$. The LSDA$+U$ calculations give a much better agreement with the observed valence-band structure, the measured electrical, and the magnetic properties. [S0163-1829(97)03732-6]

I. INTRODUCTION

Complex $3d$-transition metal oxides with the chemical formula ABO_2 (A=Li, Na,..., B=Cr, Mn, Fe, Co, Ni) and the α-$NaFeO_2$ crystal structure are of great interest as model compounds for an analysis of the rearrangement of the electronic structure of monoxides when monovalent A^{1+} ions are introduced into the crystal lattice of monoxides. In this case the formation of B^{3+} ions (with invariable O^{2-}) or O^{1-} ions (with invariable B^{2+}) is possible. Many high-energy spectral measurements of ABO_2 compounds were undertaken during the past six years which showed that $3d$ transition metal ions in $LiCrO_2$, $LiFeO_2$, or $LiCoO_2$ are trivalent, whereas Ni ions in $LiNiO_2$ are divalent.[1–7] In this respect $CuFeO_2$ can be considered as a related compound because its delafossite-type structure is indeed close to that of α-$NaFeO_2$.[8,9]

The crystal structure of $CuFeO_2$ belongs to the space group $R3m$ with $a_h=3.03$ Å and $c_h=17.09$ Å in the hexagonal description.[10] The structure, shown in Fig. 1, consists of hexagonal layers of Cu, O, and Fe with a stacking sequence of $A-B-C$ along the c axis to form a layered triangular lattice antiferromagnet, where the triangular lattices of magnetic Fe^{3+} are separated by nonmagnetic ion layers of Cu^+ and O^{2-}.[10]

Magnetic properties of $CuFeO_2$ have been intensively studied. Apostolov[11] performed Mössbauer effect and neutron diffraction measurements of $CuFeO_2$ and proposed an anti-ferromagnetic, noncollinear magnetic structure with a rhombohedral magnetic unit cell at 4.2 K. Muir and Wiedersich[12] found that $CuFeO_2$ undergoes a magnetic transition at about 19 K into an antiferromagnetic phase with a structure consisting of stacked ferromagnetic triangular planes with a collinear spin configuration along the c axis. Doumerc *et al.*[13] found the Néel temperature to be $T_N=13\,K$. At temperatures much higher than the Néel tempera-

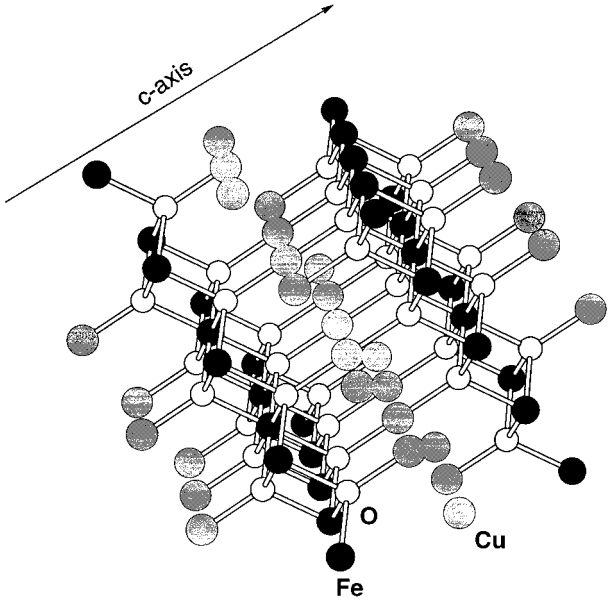

FIG. 1. Crystal structure of $CuFeO_2$. Cu atoms are denoted by large gray circles, Fe atom are denoted by dark circles, while O atoms are denoted by small empty circles.

ture, the paramagnetic susceptibility is found to obey the Curie-Weiss law.[15] Later, successive magnetic transitions at $T_{N1}=16\ K$ and $T_{N2}=11\ K$ were found from powder neutron diffraction measurements.[14,15] The magnetic structure was determined to be orthorhombic below T_{N2}. As the temperature is increased above T_{N2}, $CuFeO_2$ shows a first-order transition to a monoclinic phase.[16] The effective magnetic moment deduced from magnetic susceptibility amounts to $5.64\mu_B$,[17] whereas the powder neutron diffraction gives only $4.4\mu_B$ of the Fe^{3+} ion moment[17] which is smaller than the expected value of $5\mu_B$ for ^6S state of Fe^{3+} ions.

The optoelectronic and electrical properties of $CuFeO_2$ were investigated by Benko and Koffyberg[18,19] and Dordor *et al.*[20] $CuFeO_2$ is a semiconductor. In contrast to other delafossites, it can be made either a *p* or *n* type by suitable doping. The carrier mobility of the *p*-type samples is much higher than that of the *n*-type ones.[18,19] It was proposed that in the *p*-type material the polarons are localized on the Cu sites (forming Cu^{2+} ions), whereas in *n*-type samples they are localized on the Fe sites leading to Fe^{2+} ions.[19] The indirect allowed band gap for a *p*-type polycrystalline $CuFeO_2$ sample was found to be 1.15 eV.[18,19]

Up to now, spectral measurements and band structure calculations are absent for this compound. Its electronic properties have been discussed only on the basis of simplified bonding schemes.[19–21] Recently, a great success was achieved in crystal growth of this material, and ''perfect'' large-size single crystals (5–8 mm in diameter and 10–30 mm in length) are now available for the study of their physical properties.[22] In connection with this, we have performed XPS measurements of valence-band and core level spectra and the x-ray emission measurements of the valence spectra for all components (Cu L_α, Fe L_α, O K_α) on the specially grown single crystals of $CuFeO_2$. Also, self-consistent band structure calculations have been performed.

II. EXPERIMENT

Crystal growth of $CuFeO_2$ was carried out by a floating-zone method in an infrared radiation furnace (Type SC-48, Nichiden Machinery Ltd.). The feed rod was suspended from the upper holder by a platinum wire and the lower seed, made from a sintered rod, was fixed by a chuck. Growth was started by melting the tips of the two rods which were then brought together to form a molten zone. The feed and the seed were rotated at 30 and 15 rpm separately in opposite directions in order to promote the stirring of the melt and to equalize the heat inflow. Crystal growth was carried out by a flow (300 ml/min) of argon gas and at a growth rate in the range 0.5–1 mm/h. The hexagonal lattice constants of the crystals were determined from the x-ray diffraction patterns [$a_h=3.036(1)$ Å and $c_h=17.169(3)$ Å].

For comparison of properties we have used single crystals of FeO and CuO and a pressed tablet of $LiFeO_2$. The preparing of the latter was described earlier.[5]

The x-ray photoelectron spectra were measured on an ESCA spectrometer from Physical Electronics (PHI 5600 ci) using monochromatic Al $K\alpha$ radiation. The single crystal of $CuFeO_2$ was investigated after having broken vacuum. The spectra were calibrated using an Au foil [$E_B(4f_{7/2})=84.0$ eV]. The energy resolution as determined at the Fermi level of an Au-foil was approximately 0.4 eV.

The Cu $L\alpha$ ($3d4s\rightarrow 2p_{3/2}$ transition), Fe L_α ($3d4s\rightarrow 2p_{3/2}$ transition), and O $K\alpha$ ($2p\rightarrow 1s$ transition) x-ray emission spectra (XES) were measured on an RSM-500 x-ray spectrometer with electron excitation. The Fe $L\alpha$ and Cu $L\alpha$ spectra were obtained in the second-order reflection with a broadening of approximately 0.4 and 0.8 eV, respectively.

The O $K\alpha$ spectrum was measured in first-order reflection with a broadening of 0.6 eV. To calibrate the Cu $L\alpha$, Fe $L\alpha$, and O $K\alpha$ spectra we used the $L\alpha$ spectra of pure Cu, Fe, and V (929.7, 705.0, and 511.3 eV, respectively). The x-ray tube was operated at $V=4$ keV and $i=0.3$ mA.

The x-ray emission spectra were brought to the scale of the binding energies with respect to the Fermi level using the binding energies of relevant initial (core level) states of the x-ray transitions as measured by the X-ray photoelectron spectroscopy (XPS) technique. Corresponding binding energies are $E_B(\text{Cu } 2p_{3/2})=932.4$ eV, $E_B(\text{Fe } 2p_{3/2})=711.5$ eV, and $E_B(\text{O } 1s)=530.05$ eV.

III. COMPUTATIONAL DETAILS

Calculations of the electronic structure of $CuFeO_2$ were performed using two approximations for the interelectron Coulomb interaction: conventional local spin density approximation (LSDA), and an LSDA+U approach.[31,32] LSDA calculations were performed using the full-potential linearized augmented plane wave method (FP-LAPW) as well as the linearized muffin-tin orbitals in the atomic sphere approximation (LMTO-ASA) method. LSDA+U calculations were carried out using the LMTO-ASA method.

For $CuFeO_2$ we used a cell dimension of $a_h=3.03$ Å and $c_h=17.09$ Å. The unit cell (one formula unit) contains four atoms: in terms of the primitive translation vectors, the Cu atom sits in the (0,0,0) position, the Fe and two O atoms occupy the positions $(\frac{1}{2},\frac{1}{2},\frac{1}{2})$, $(\frac{1}{9},\frac{1}{9},\frac{1}{9})$ and $(\frac{8}{9},\frac{8}{9},\frac{8}{9})$, respectively (Fig. 1). In this configuration, the copper has a linear twofold oxygen coordination, the iron is coordinated to six oxygen atoms in a distorted octahedron, and the oxygen atom is surrounded by a tetrahedron of three Fe atoms and one Cu atom.

We calculated the electronic structures of $CuFeO_2$ using the LSDA (Ref. 23) based FP-LAPW method,[24,25] in which we used the spin-polarized version of the exchange-correlation potential of Ceperley and Alder,[26] as parametrized by Perdew and Zunger.[27] The core states were treated fully relativistically, while the valence states were treated semirelativistically (without spin-orbit interaction, which plays a relatively minor role here). No shape approximation was made for either the potential or the charge density. The chosen muffin-tin sphere radii are 1.111, 1.191, and 0.794 Å for Cu, Fe, and O, respectively. The nonspherical charge density and potential were expanded in terms of lattice harmonics of angular momentum $l\leqslant 8$ inside the muffin-tin spheres and were expanded in more than 7900 plane waves in the interstitial region. A basis set of about ~190 FP-LAPW's/atom were used. During the self-consistency cycle, the Brillouin zone (BZ) integration was performed using 28 special **k** points[28] in the irreducible BZ. The total density of states (DOS) and site-decomposed local DOS (LDOS, within

the muffin-tin sphere) were calculated using the tetrahedron method,[29,30] and the extrapolation of the energy eigenvalues in 189 **k** points were directly calculated using the FP-LAPW method.

The electronic structure of $CuFeO_2$ was also calculated by the LMTO-ASA method in the LSDA+U approximation, in order to take into account Coulomb correlations between d electrons of transition metal ions. The LMTO-ASA method was also used in the LSDA approach and gave results very similar to FP-LAPW results.

We used LSDA+U functional as follows:[31,32]

$$E^{\mathrm{LSDA}+U}[\rho^{\sigma}(\mathbf{r}),\{n^{\sigma}\}]=E^{\mathrm{LSDA}}[\rho^{\sigma}(\mathbf{r})]+E^{\mathrm{U}}[\{n^{\sigma}\}]-E_{dc}[\{n^{\sigma}\}], \tag{1}$$

where $\rho^{\sigma}(\mathbf{r})$ is the charge density for spin-σ electrons and $E^{\mathrm{LSDA}}[\rho^{\sigma}(\mathbf{r})]$ is the standard LSDA functional. Equation (1) asserts that the LSDA is a sufficient approximation in the absence of orbital polarizations, while the latter are described by a theory of a mean-field (Hartree-Fock) type:

$$E^{\mathrm{U}}[\{n\}]=\tfrac{1}{2}\sum_{\{m\},\sigma}\{\langle m,m''|V_{ee}|m',m'''\rangle n^{\sigma}_{mm'}n^{-\sigma}_{m''m'''}+(\langle m,m''|V_{ee}|m',m'''\rangle-\langle m,m''|V_{ee}|m''',m'\rangle)n^{\sigma}_{mm'}n^{\sigma}_{m''m'''}\}, \tag{2}$$

where V_{ee} are the screened Coulomb interactions between the nl electrons. Finally, the last term in Eq. (2) corrects for double counting [in the absence of orbital polarizations, Eq. (2) should reduce to the E^{LSDA}] and is given by

$$E_{dc}[\{n^{\sigma}\}]=\frac{1}{2}\,Un(n-1)-\frac{1}{2}\,J[n^{\uparrow}(n^{\uparrow}-1)+n^{\downarrow}(n^{\downarrow}-1)], \tag{3}$$

where $n^{\sigma}=\mathrm{Tr}(n^{\sigma}_{mm'})$ and $n=n^{\uparrow}+n^{\downarrow}$. U and J are the screened Coulomb and exchange parameters.[33]

In addition to the usual LSDA potential, the effective single-particle potentials used in the effective single-particle Hamiltonian H (LSDA+U potential correction) were

$$V^{\sigma}_{mm'}=\sum_{m''m'''}\{\langle m,m''|V_{ee}|m',m'''\rangle n^{-\sigma}_{m''m'''}+(\langle m,m''|V_{ee}|m',m'''\rangle-\langle m,m''|V_{ee}|m''',m'\rangle)n^{\sigma}_{m''m'''}\}-U\left(n-\frac{1}{2}\right)+J\left(n^{\sigma}-\frac{1}{2}\right). \tag{4}$$

The matrix elements V_{ee} can be expressed in terms of complex spherical harmonics and effective Slater integrals F^k as[34]

$$\langle m,m''|V_{ee}|m',m'''\rangle=\sum_{k}\,a_k(m,m',m'',m''')F^k, \tag{5}$$

where $0\leqslant k\leqslant 2l$, and,

$$a_k(m,m',m'',m''')=\frac{4\pi}{2k+1}\sum_{q=-k}^{k}\langle lm|Y_{kq}|lm'\rangle\times\langle lm''|Y^{*}_{kq}|lm'''\rangle.$$

If the $|lm'\rangle$ basis consists of complex spherical harmonics,

$$a_k(m,m',m'',m''')=\sum_{q=-k}^{k}(2l+1)^2(-1)^{m+q+m'}\times\begin{pmatrix} l & k & l\\ 0 & 0 & 0\end{pmatrix}^2\begin{pmatrix} l & k & l\\ -m & q & m'\end{pmatrix}\times\begin{pmatrix} l & k & l\\ -m'' & -q & m'''\end{pmatrix}. \tag{6}$$

For d electrons, one needs F^0, F^2, and F^4 and these can be linked to the Coulomb and Stoner parameters obtained from the LSDA-supercell procedures via $U=F^0$ and $J=(F^2+F^4)/14$, while the ratio F^4/F^2 is constant ($\sim$0.625) to a good accuracy for $3d$ elements.[35,36] For $CuFeO_2$ we find $U=8.0$ eV, $J=0.9$ eV for Fe and Cu. The ASA radii were chosen as follows: 1.11 Å for O and 1.59 Å for Cu and Fe.

Historically the cluster configuration interaction method[37–39] was the first to be used in attempts to include strong Coulomb interactions in electronic structure calculations. While being superior to our one-electron LSDA+U method as a fully many-electron approach, the cluster method is too oversimplified in the sense that it models a crystal by a nearest neighbors cluster of atoms, while the LSDA+U method properly takes into account all interactions between all atoms in crystal.

IV. RESULTS AND DISCUSSION

A. Core level spectra

It is well known that x-ray photoelectron core level spectra give important information on the electronic states of the materials under considerations. It is generally accepted that the simple *charge-transfer* model described by van der Laan *et al.*[40] and Zaanen *et al.*[41] is a good approximation for the interpretation of $2p$ x-ray photoelectron spectra of transition metal compounds.

The Cu $2p$ x-ray photoelectron spectra of $CuFeO_2$ and CuO are shown in Fig. 2. The spectrum of CuO exhibits an intense satellite on the high binding energy side at about 9 eV above the main peak. The satellite line corresponds to the $2p^{-1}3d^{9}$ final state, while the main line corresponds to the $2p^{-1}3d^{10}L^{-1}$ final state. Here, L^{-1} denotes a hole on a ligand atom after the so-called charge-transfer process. The structure seen in the satellite line is due to the multiplet splitting in the $2p^{5}3d^{9}$ final state.

The Cu $2p_{3/2}$ spectrum of $CuFeO_2$ has only one peak at 932.5 eV which is significantly narrower than the main peak of CuO. Note that the Cu $2p$ spectrum of $CuFeO_2$ is similar

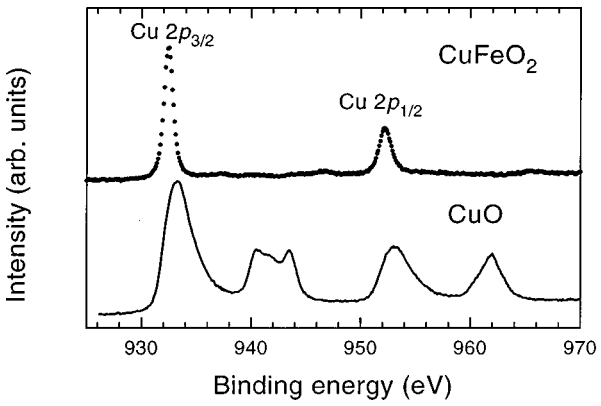

FIG. 2. Cu $2p$ x-ray photoelectron spectra of $CuFeO_2$ and CuO.

to that of Cu_2O (Ref. 42) where copper ions have a formal valency $+1$. The Cu $2p$ spectrum of $CuFeO_2$ shows no multiplet splitting as expected for a full Cu $3d$ shell. Therefore, the ground state of the copper ions in $CuFeO_2$ consists mainly of the configuration $3d^{10}$, resulting in a single core level peak with the configuration $2p^{-1}3d^{10}$.

The energy difference between the Cu $2p$ binding energies of CuO and $CuFeO_2$ indicates the presence of different valence states of these oxides. It is known that Cu^{1+} compounds exhibit a Cu $2p$ spectra with lesser binding energies than Cu^{2+} compounds. This is a further proof of the $3d^{10}$ ground state configuration of Cu in $CuFeO_2$.

Figure 3 shows the Fe $2p$ x-ray photoelectron spectra of $CuFeO_2$, $LiFeO_2$, and FeO. In accordance with our work,[5] the ground state configuration of the Fe cation in $LiFeO_2$ is $3d^5$. On the other hand, as indicated by other investigators,[43–45] the ground state configuration of Fe in FeO is $3d^6$. The Fe $2p_{3/2,1/2}$ spectra for all oxides of this work show strong satellite structure which corresponds to a shake-up satellite. Whereas the Fe $2p_{3/2,1/2}$ main lines for FeO correspond to well screened $2p^{-1}3d^7L^{-1}$ final states, the satellites are described as poorly screened $2p^{-1}3d^6$ final states. For $LiFeO_2$, the main lines are assigned to the $2p^{-1}3d^6L^{-1}$ final states, and the satellites are assigned to

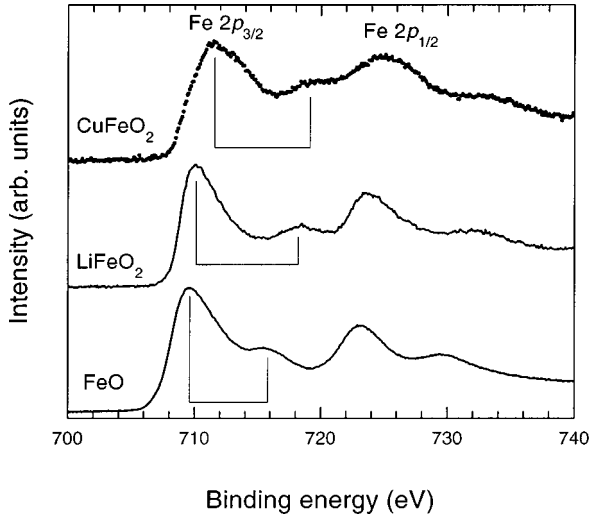

FIG. 3. Fe $2p$ x-ray photoelectron spectra of $CuFeO_2$, $LiFeO_2$, and FeO.

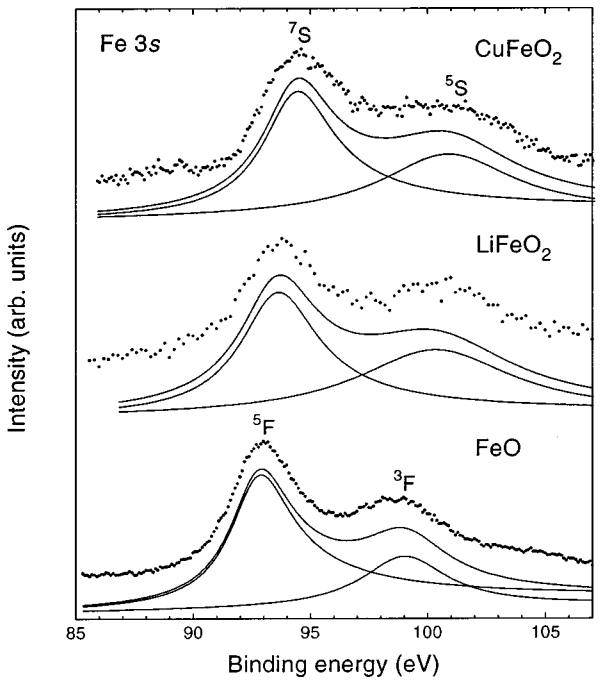

FIG. 4. Fe $3s$ x-ray photoelectron spectra of $CuFeO_2$, $LiFeO_2$, and FeO.

the $2p^{-1}3d^5$ final states. The energy separation between the main lines and the satellites for $CuFeO_2$ is closer to that of $LiFeO_2$ than to FeO. This shows that Fe ions in $CuFeO_2$ are trivalent, as they are in $LiFeO_2$.

The Fe $2p$ spectra of $CuFeO_2$ are partly distorted as a result of the superposition with Cu $L_2M_{2,3}M_{2,3}$ and $L_3M_{2,3}M_{2,3}$ Auger spectra. This is why the Fe $2p$ spectra of $CuFeO_2$ are broader than those of $LiFeO_2$ and FeO.

The $3s$ core levels of the $3d$ transition metals are known to exhibit exchange splitting. The magnitude of the splitting is proportional to $(2S+1)$, where S is a local $3d$ spin in the ground state. In addition to the exchange interaction between $3d$ and $3s$ states, an account must be taken of the *charge-transfer* process. For Cu oxides, the *charge-transfer* effect dominates the multiplet effect in the $3s$ spectra.[46] As the number of d electrons decreases, the role of charge-transfer processes becomes less important and in Mn compounds the $3s$ splitting is mainly determined by exchange processes.[47,48]

In Fig. 4, the Fe $3s$ core level spectra of $CuFeO_2$, $LiFeO_2$, and FeO are shown. The magnitude of the Fe $3s$ splitting in $CuFeO_2$ is equal to 6.5 eV. The same splitting was found for $LiFeO_2$, with the high-spin $3d^5$ configuration $(S=\frac{5}{2})$ of Fe^{3+} ions in the ground state. For FeO with $S=2$, the exchange splitting is less. Therefore we can conclude that the high-spin state $S=\frac{5}{2}$ for Fe^{3+} ions is realized in $CuFeO_2$.

B. Band structure calculations

The results of the LSDA calculation are presented in Figs. 5(a) and 5(b) (FP-LAPW and LMTO-ASA, respectively). One can see that the O $2p$ band is centered approximately at 6 eV below the Fermi level with a bandwidth of approximately 5 eV. The completely filled Cu $3d$ band is centered at approximately -2 eV. The narrow band formed by the Fe

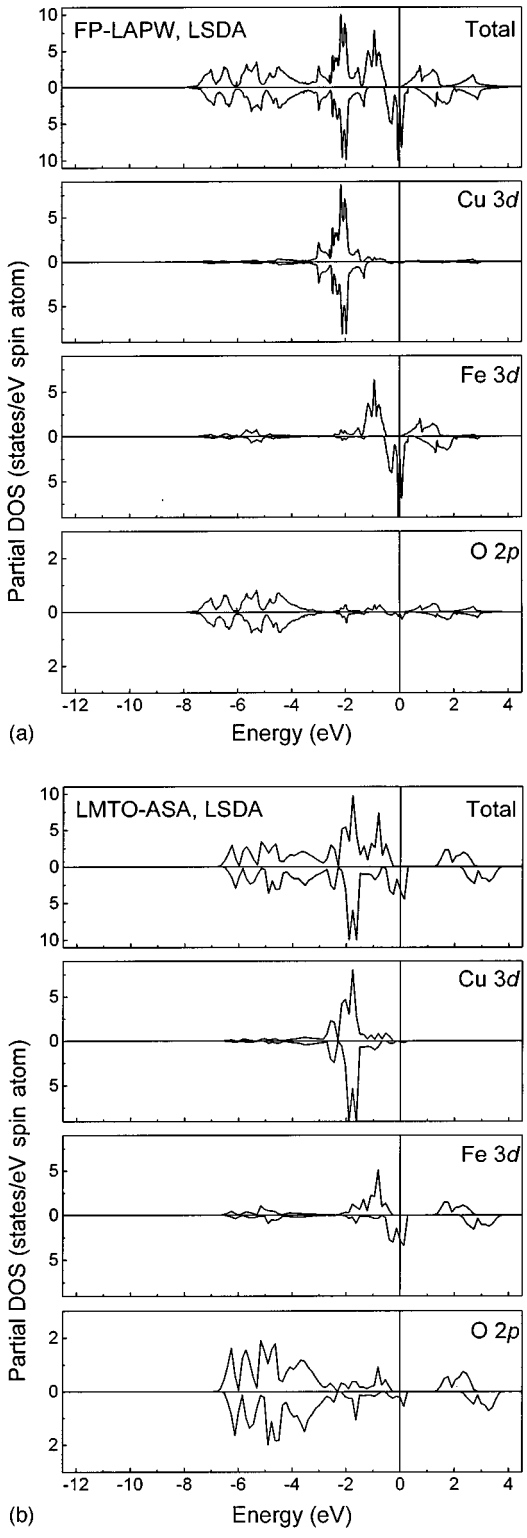

FIG. 5. (a) Total and partial densities of states calculated using the LSDA approximation (FP-LAPW method); (b) densities of states calculated using the LSDA approximation (LMTO-ASA method). Total DOS is given in states/eV spin cell.

$t_{2g\uparrow}^3$ electrons is placed at about 1 eV below the Fermi energy. The Fe $t_{2g\downarrow}$ band crosses the Fermi level and is two-thirds filled (it is for this reason that the magnetic moment is small). The Fe $e_{g\uparrow}$ and $e_{g\downarrow}$ bands are empty and are placed at

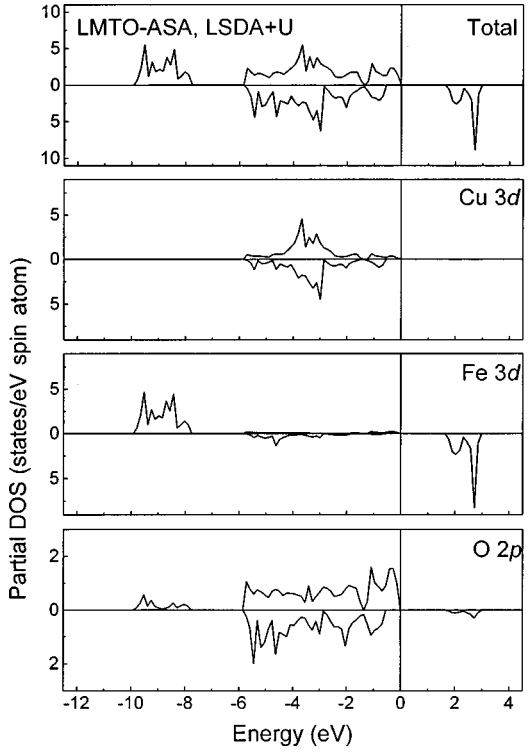

FIG. 6. Total and partial densities of states calculated using the LSDA+U approximation. Total DOS is given in states/eV spin cell.

approximately 1 and 2 eV above the Fermi level, respectively. Therefore, the Cu $3d$ band is located 1 eV lower than the Fe $3d$ band.

According to the LSDA calculations, $CuFeO_2$ is a metal where Fe ions are in the low-spin state and the magnetic moment is equal to $0.96\mu_B$ (FP-LAPW method). The LMTO-ASA calculation gives a magnetic moment of $0.91\mu_B$.

These results contradict the experimental results which show that $CuFeO_2$ is a semiconductor with a gap of 1.15 eV.[18,19] From the neutron diffraction study, the Fe^{3+} ion moment in $CuFeO_2$ is equal to 4.4 μ_B[17] which corresponds to a high-spin state of the Fe^{3+} ions. The experiment also shows that the Fe $3d$ states are situated deeper relative to the Fermi level than the Cu $3d$ states.

We believe that these incorrect theoretical results arise from the failure of LSDA to properly take into account the on-site Coulomb correlation between d electrons of transition metal ions. Therefore, we must take into account the Coulomb correlation function U and calculate the electronic structure of $CuFeO_2$ using the LSDA+U approach.

Figure 6 shows the partial densities of state for $CuFeO_2$ calculated in the LSDA+U approach. As a result of the LSDA+U calculation we have obtained the result that $CuFeO_2$ is a semiconductor with the band gap of 2.0 eV which corresponds closer to the measured one. The broad O $2p$ band is centered at approximately 5 eV below the Fermi level. The Cu $3d$ band is filled completely and located in the same energy area. The Fe $3d_\uparrow$ ($t_{2g\uparrow}^3$ and $e_{g\uparrow}^2$) states are placed at about 9 eV below E_F. The Fe $3d_\downarrow$ band is nearly empty and thus Fe ions are mostly in the majority spin state.

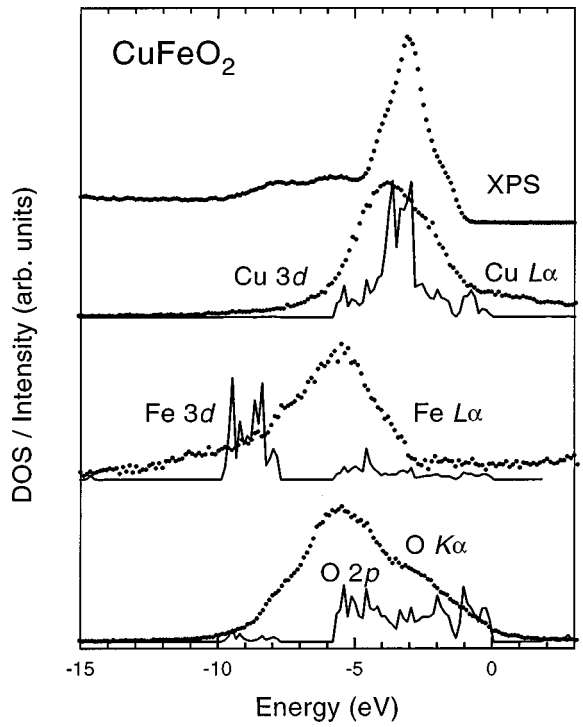

FIG. 7. X-ray photoelectron spectrum of the valence bands and Cu $L\alpha$, Fe $L\alpha$, and O $K\alpha$ x-ray emission spectra of $CuFeO_2$ as compared with partial densities of states calculated using the LSDA+U approximation. X-ray emission spectra are brought to a common energy scale using the core level electron binding energies.

The magnetic moment is equal to $3.76\mu_B$ [in accordance with $\mu_{\text{eff}}=4.65\,\mu_B$ determined as $\mu_{\text{eff}}=2\sqrt{S(S+1)}$]. It is also seen that the Cu $3d$ band is placed 5 eV higher than the Fe $3d$ one.

C. Valence-band spectra

Figure 7 shows the valence-band x-ray photoemission spectrum and the Cu $L\alpha$, Fe $L\alpha$, and O $K\alpha$ x-ray emission spectra of $CuFeO_2$ together with the partial densities of occupied (spin up plus spin down) states from the LSDA+U calculations. The x-ray emission spectra are arranged with respect to the Fermi level, taking into account the Cu $2p_{3/2}$, Fe $2p_{3/2}$, and O $1s$ core level binding energies measured by means of x-ray photoelectron spectroscopy (XPS). For $CuFeO_2$ the Cu $L\alpha$ emission band lies at about -3.6 eV and this value agrees well with the main peak of the XPS valence-band spectrum situated near the Fermi level with the maximum at -3 eV. It is interesting, that the shape of the XPS spectrum of $CuFeO_2$ is similar to that of Cu_2O and consistent with our interpretation that copper is in the 1+ state. The valence band XPS spectrum can be found in the work by Ghijsen *et al.*[42]

For the Al $K\alpha$ excitation, the cross section ratio $\sigma(\text{Cu }3d)$: $\sigma(\text{Fe }3d)$:$\sigma(\text{O }2p)$ is equal to 1:0.18:0.02 (Ref. 49) and as a consequence, the main XPS peak at the binding energy of -3 eV results from Cu $3d$ states. This is why we compare the x-ray photoelectron and Cu $L\alpha$ spectra with the Cu $3d$ partial density of states. We bring the Cu $3d$ partial density of states into coincidence with the position of the main maximum of the XPS valence-band spectrum. The general width and shape of the XPS spectrum agrees well with the calculated Cu $3d$ density of states. The states near the Fermi level are represented both in the XPS valence band spectrum and in the Cu $3d$ partial density of states. According to the LSDA+U calculation, these states are determined as the Cu $3d$–O $2p$ hybridized states.

Fe $3d$ states are given in the Fe $L\alpha$ spectrum. There is a discrepancy between the location of the calculated and measured Fe $3d$ states. In accordance with the LSDA+U calculations, the Fe $3d$ states are formed mainly in the energy area between -8 and -10 eV, whereas the measured ones have a maximum at -5.3 eV. It is known that one-particle (band structure) calculations are unable to give a correct description of the $3d$ electronic states because of electron-electron correlations. For Fe $3d$ electrons, the electron-electron correlations are rather strong, as one can see from the high intensity of the Fe $2p$ satellite (see Fig. 3). Perhaps, the Coulomb parameter U calculated in the supercell approximation[33] is actually too large and leads to deepening Fe $3d$ states relative to the measured ones. A smaller value of U would give better agreement with the spectral data. Note that the relative positions of the Cu $3d$ and O $2p$ bands are reproduced well by the LSDA+U method but not by the LSDA method.

The LSDA+U method takes into account electron correlation on the simplest possible mean-field level, and being a one-electron approximation, it cannot properly describe complicated many-electron effects caused by the presence of the core hole in x-ray spectroscopy. In such a case the cluster configuration interaction method[32–39] is more appropriate.

The Fe $3d$ states are substantially hybridized with the O $2p$ states which follows from energy overlapping of the Fe $3d$ and O $2p$ states. The O $2p$ states are concentrated at 1–10 eV with the maximum at 5.4 eV, as one can see from the position of the O $K\alpha$ x-ray emission spectrum in the binding energy scale. The component O $2p$ DOS is also shown here. The O $2p$ states are strongly hybridized with the Fe $3d$ states, as one sees from the coincidence of the O $K\alpha$ and Fe $L\alpha$ x-ray spectra in the common energy scale. Note that the similar effect was found for the $LiFeO_2$ oxides.[5] In contrast to $LiFeO_2$, the Fe $3d$ and O $2p$ states lie deeper relative to the Fermi level and probably do not affect the conduction properties of the $CuFeO_2$ oxide. A similar conclusion was made by Benko and Koffyberg[18] since substitutions of a Fe^{3+} ion by other 3+ ions do not change the value of the band gap.

V. CONCLUSION

In summary, we have presented x-ray photoemission and soft x-ray emission spectra of all the components of $CuFeO_2$ in combination with the results of *ab initio* LSDA and LSDA+U calculations. Using the spectral measurements we have shown that Cu ions are in the 1+ valence state and Fe^{3+} ions are in the high-spin configuration $S=5/2$. It is found, that the experimental maxima of the Cu $3d$, Fe $3d$, and O $2p$ bands lie at -3.0, -5.3, -5.4 eV relative to the Fermi level, respectively.

The LSDA calculations contradict the experimental results and do not correctly describe the component band po-

sitions for $CuFeO_2$ on the energy scale relative to the Fermi level. Moreover, according to the LSDA calculations, $CuFeO_2$ is a metal with the conducting electrons at E_F being Fe-like ions in the low-spin state and a magnetic moment of about $0.91-0.96\ \mu_B$, which is also in contradiction with the experimental data whereby $CuFeO_2$ is a semiconductor with a band gap of 1.15 eV and a magnetic moment of $4.4\mu_B$. It is shown that this contradiction arises from the failure of LSDA to take into account the on-site Coulomb correlations between d electrons of the transition metal ions.

Our LSDA$+U$ calculations removed these contradictions and showed that (a) $CuFeO_2$ is a semiconductor (band gap of 2.0 eV) with Fe^{3+} ions in the high-spin configuration $S=5/2$ with a magnetic moment of $3.76\mu_B$; and (b) the Cu $3d$ band is placed above the Fe $3d$ band with respect to the Fermi level which is in accord with the XPS and XES measurements. The energy positions of the components as predicted by the LSDA$+U$ method correspond closer to the ones found by the XPS and XES methods. For the complete Cu $3d$ shell, the agreement between the experiments and the one-particle theory is very good, although some discrepancy remains for the positions of the Fe $3d$ and O $2p$ states.

For the highly correlated Fe $3d$ electrons, there is a contradiction between the theoretically predicted Fe $3d$ position and the experimentally measured one. Many body effects must be taken into account.

ACKNOWLEDGMENTS

Financial supports from the NATO Project (Grant No. HTECH.LG940861), the International Project ''Electron Structure of Oxides,'' the Russian Foundation for Fundamental Research (Grant No. 96-03-32092), and the Campus Laboratory Collaboration Program of the University of California are gratefully acknowledged.

[1] P. Kuiper, G. Kruizinga, J. Ghijsen, G. A. Sawatzky, and H. Verweij, Phys. Rev. Lett. **62**, 221 (1989).
[2] J. van Elp, J. L. Wieland, H. Eskes, P. Kuiper, G. A. Sawatzky, F. M. F. de Groot, and T. S. Turner, Phys. Rev. B **44**, 6090 (1991).
[3] J. van Elp, H. Eskes, P. Kuiper, and G. A. Sawatzky, Phys. Rev. B **45**, 1612 (1992).
[4] F. M. F. de Groot, Ph. D. thesis, University of Nijmegen, 1991.
[5] V. R. Galakhov, E. Z. Kurmaev, M. Neumann, D. G. Kellerman, V. S. Gorshkov and St. Uhlenbrock, Solid State Commun. **95**, 347 (1995).
[6] V. R. Galakhov, E. Z. Kurmaev, St. Uhlenbrock, M. Neumann, D. G. Kellerman, and V. S. Gorshkov, Solid State Commun. **99**, 221 (1996).
[7] D. G. Kellerman, V. S. Gorshkov, V. G. Zubkov, V. A. Perelyaev, V. R. Galakhov, E. Z. Kurmaev, S. Uhlenbrock, and M. Neumann, J. Inorg. Chem. (to be published).
[8] C. T. Prewitt, R. D. Shannon, and D. B. Roggers, Inorg. Chem. **10**, 719 (1971).
[9] J. P. Doumerc, A. Ammar, A. Wichainchai, M. Pouchard, and P. Hagenmuller, J. Phys. Chem. Solids **48**, 37 (1987).
[10] A. Pabst, Am. Mineral. **75**, 105 (1988).
[11] A. Apostolov, God. Sofii Univ. **59**, 47 (1966); C. R. Acad. Burg. Sci. **22**, 65 (1969).
[12] A. H. Muir, Jr. and H. Wiedersich, J. Phys. Chem. Solids **28**, 65 (1967).
[13] J. P. Doumerc, A. Wichainchai, A. Ammar, M. Pouchard, and P. Hagemuller, Mater. Res. Bull. **21**, 745 (1986).
[14] S. Mitsuda, H. Yosizawa, N. Yaguchi, and M. Mekata, J. Phys. Soc. Jpn. **60**, 1885 (1991).
[15] M. Mekata, N. Yaguchi, T. Takagi, S. Mitsuda, and H. Yoshizawa, J. Magn. Magn. Mater. **104–107**, 823 (1992).
[16] K. Takeda, K. Miyake, M. Hitaka, T. Kawae, N. Yaguchi, and M. Mekata, J. Phys. Soc. Jpn. **63**, 2017 (1994).
[17] M. Mekata, N. Yaguchi, T. Takagi, T. Sugino, S. Mitsuda, H. Yoshizawa, N. Hosoito, and T. Shinjo, J. Phys. Soc. Jpn. **62**, 4474 (1993).
[18] F. A. Benko and F. P. Koffyberg, J. Phys. Chem. Solids **45**, 57 (1984); Can. J. Phys. **63**, 1306 (1985); Phys. Status Solidi **94**, 231 (1986).
[19] F. A. Benko and F. P. Koffyberg, J. Phys. Chem. Solids **48**, 431 (1987).
[20] P. Dordor, J. P. Chaminade, A. Wichainchai, E. Marquestaut, J. P. Doumerc, M. Pouchard, P. Hagenmuller, and A. Ammar, J. Solid State Chem. **75**, 105 (1988).
[21] D. B. Rogers, R. D. Shannon, C. T. Prewitt, and J. L. Gillson, Inorg. Chem. **10**, 723 (1971).
[22] T.-R. Zhao, M. Hasegawa, M. Koike, and H. Takei, J. Cryst. Growth **148**, 189 (1995).
[23] P. Hohenberg and W. Kohn, Phys. Rev. **136**, B864 (1964); W. Kohn and L. J. Sham, Phys. Rev. **140**, A1 133 (1965).
[24] O. K. Andersen, Phys. Rev. B **12**, 3060 (1975); E. Wimmer, H. Krakauer, M. Weinert, and A. J. Freeman, *ibid.* **24,** 864 (1981); D. R. Hamann, Phys. Rev. Lett. **42,** 662 (1979); S.-H. Wei and H. Krakauer, *ibid.* **55,** 1200 (1985); S.-H. Wei, H. Krakauer, and M. Weinert, *ibid.* **32,** 7792 (1985).
[25] D. J. Singh, *Planewaves, Pseudopotentials, and the LAPW Method* Kluwer, Boston, 1994).
[26] D. M. Ceperley and B. J. Alder, Phys. Rev. Lett. **45,** 566 (1980).
[27] J. P. Perdew and A. Zunger, Phys. Rev. B **23**, 5048 (1981)
[28] H. J. Monkhorst and J. D. Pack, Phys. Rev. B **13**, 5188 (1976).
[29] G. Lehmann, P. Rennert, M. Taut, and H. Wonn, Phys. Status Solidi **37**, K27 (1970); G. Lehmann and M. Taut, *ibid.* **54**, 469 (1972).
[30] O. Jepsen and O. K. Andersen, Solid State Commun. **9**, 1763 (1971).
[31] V. I. Anisimov, J. Zaanen, and O. K. Andersen, Phys. Rev. B **44**, 943 (1991).
[32] A. I. Liechtenstein, V. I. Anisimov, and J. Zaanen, Phys. Rev. B **52**, R5 467 (1995)
[33] V. I. Anisimov and O. Gunnarsson, Phys. Rev. B **43**, 7570 (1991).
[34] B. R. Judd, *Operator Techniques in Atomic Spectroscopy* (McGraw-Hill, New York, 1963).
[35] V. I. Anisimov, I. V. Solovyev, M. A. Korotin, M. T. Czyzyk, and G. A. Sawatzky, Phys. Rev. B **48**, 16 929 (1993).
[36] F. M. F. de Groot, J. C. Fuggle, B. T. Thole, and G. A. Sawatzky, Phys. Rev. B **42**, 5459 (1990).
[37] A. Fujimori and F. Minami, Phys. Rev. B **30**, 957 (1984).

[38] J. Zaanen, G. A. Sawatzky, and J. W. Allen, Phys. Rev. Lett. **55**, 418 (1985).
[39] S. Hüfner, Z. Phys. B **61**, 135 (1985).
[40] G. van der Laan, C. Westra, C. Haas, and G. A. Sawatzky, Phys. Rev. B **23,** 4369 (1981).
[41] J. Zaanen, C. Westra, and G. A. Sawatzky, Phys. Rev. B **33,** 8060 (1986).
[42] J. Ghijsen, L. H. Tjeng, J. van Elp, H. Eskes, J. Westerink, G. A. Sawatzky, and M. T. Czyzyk, Phys. Rev. B **38,** 11 322 (1988).
[43] A. Fujimori, M. Saeki, N. Kimizuka, M. Taniguchi, and S. Suga, Phys. Rev. B **34,** 7318 (1986).
[44] J. Lad and V. E. Henrich, Phys. Rev. B **38,** 10 860 (1988).
[45] G. Lee and S.-J. Oh, Phys. Rev. B **43,** 14 674 (1991).
[46] T. Mizokawa, A. Fujimori, H. Namatame, K. Akeyama, and N. Kosugi, Phys. Rev. B **49,** 7193 (1994).
[47] K. Okada and A. Kotani (unpublished). K. Okada and A. Kotani, J. Phys. Soc. Jpn. **61,** 4619 (1992); K. Okada, A. Kotani, and B. Thole, J. Electron Spectrosc. Relat. Phenom. **58,** 325 (1992).
[48] T. Uozumi, K. Okada, A. Kotani, R. Zimmermann, P. Steiner, S. Hüfner, Y. Tezuka, and S. Shin (unpublished).
[49] J. J. Yeh and I. Lindau, At. Data Nucl. Data Tables **32,** 1 (1985).